Australian Journal of Basic and Applied Sciences, 5(5): 943-954, 2011
ISSN 1991-8178

Effect of Gas Channel Geometry on Performance of Pem Fuel Cells

S. Majidyfar, I. Mirzaie, S. Rezazadeh, P. Mohajeri Khameneh, H. Oryani

Department of Mechanical Engineering, Faculty of Engineering, Urmia University, Urmia, 57169-33111, Iran.

Abstract: A three-dimensional computational model was developed to investigate the performance of a polymer electrolyte fuel cell with straight channels. The proposed model was single domain and both of the anode and the cathode humidifications were involved in the domain. Two geometries with rectangular and trapezoidal channel configuration were simulated and the obtained results in a low cell voltage (which leads to high current densities in two geometries) were compared. Similar boundary conditions employed in two geometries. The geometry with rectangular channel cross-section experienced higher current density than the other geometry. Anode and cathode concentration losses and ohmic loss were calculated for two cases. Larger interface between flow channel and gas diffusion layer in the trapezoidal case led to a better diffusion of the reactants over the reacting area and as a result of that concentration losses decreased, but ohmic loss became higher in this case.

Key words: PEMFC; CFD; Channel geometry; Overpotential.

INTRODUCTION

Fuel cells are electrochemical devices that convert chemical energy of reactants, directly into electrical energy. Different types of fuel cells has been developed, which are distinguished by the electrolyte used. Among all kinds of fuel cells, proton exchange membrane (PEMFCs) has been considered as a prime candidate for future transportation application as well as for small devices such as laptop computers. Fuel cell systems need more improvement in order to become commercially used, because their expense is still too high. Some advantages of the PEMFC are low temperature operation, easy startup, zero emission, high efficiency. The geometry of the fuel cell considered in this study is presented in figure1.

In recent years, modeling and simulation of different aspects in PEMFCS are being used widely in researches with a view to enhancing the cell performance. To obtain a high performance, voltage losses of the cell such as activation losses, ohmic losses, and concentration losses must be reduced. Some voltage difference from equilibrium is needed to generate current from a fuel cell. These losses are called activation losses that are influenced by temperature, pressure, mole fraction of reactants, and catalyst materials. The mole fractions of reactants are depended on the mass transport in the flow channel and the gas diffusion layer (GDL). Concentration losses are associated with the procedure of the preparing reactants and removing products, thus concentration losses and activation losses are partially depended on each other (O'Hayre, 2006). Ohmic losses take place because of resistance to the flow of the ions in the membrane and resistance to the flow of electrons through the electrically conductive fuel cell components (Barbir, R., 2005).

It is well established the magnitude of the cathode overpotential is much higher than the anode overpotential (Larminie, 2003). The intricacy of oxygen diffusion and water removal and also larger activation losses in the cathode side leads to higher concentration losses. Importance of humidity in decreasing the ohmic losses has been declared in several researches. Springer *et al*. (1991) calculated membrane conductivity for a 117 Nafion membrane in different humidities. Buchi and Scherer (2001) examined the effect of humidity at both electrodes. Their result showed that when the membrane thickness is less than $50\mu m$, the anode humidification is more important than the cathode humidification in order to decrease ohmic loss. In order to improve the cell performance, the reactants diffusion should be facilitated. Different channel configurations and flow modes have been used to improve the cell performance (Ge, 2003; Sun, 2006; Chiang, 2006; Guvelioglu, 2005). Ge and Yi (2003) investigated the effect of co-flow mode and counter-flow mode in straight gas channels. Their result showed that Counter-flow mode produce better operation when the inlet gases were used

Corresponding Author: S. Majidyfar, Department of Mechanical Engineering, Faculty of Engineering, Urmia University, Urmia, 57169-33111, Iran.
Tel/fax:+98-241-5237618; Mob: +98-937-470-6343
E-mail: samad_majidyfar@yahoo.com

with low humidity. In the both flow mode for the high humidity inlet gases, the increase in the membrane conductivity leads to higher cathode overpotential because of attendance of liquid water. But for low humidity inlet gases, co-flow mode leads to membrane dehydration. In this case Counter-flow mode let for the internal humidification of the gas steams. Sun *et al*. (2006) developed a numerical study, which suggested using a trapezoidal channel cross-section instead of a rectangular or square cross-section to improve cell performance. Chiang and Chu (2006) developed a three dimensional model for a PEMFC with various channel geometrical parameters (channel width, length, and height). It was found that flat channels gave higher performance. Guvelioglu and Stenger (2005) conducted a numerical simulation for a two dimensional PEMFC with different channel and shoulder widths. The channel-shoulder width ratio was maintained constant in their study. Their results showed that the geometries with smaller channel and shoulder widths improve the cell performance.

In the present study, a three-dimensional model with straight channels in the anode and cathode sides was used for the computational analysis. Simulations were performed for two different channel cross-sections (rectangular and trapezoidal), while the same mass flow rates of the reactants and inlet boundary conditions were maintained for the both configurations. Ohmic losses, anode and cathode overpotentials were calculated at a low cell voltage in order to clarify the real scenario of the cell performance. Also membrane conductivity, temperature and oxygen mole fraction were computed, because voltage losses were related to them. The simulation results were validated by comparison with results in the literature.

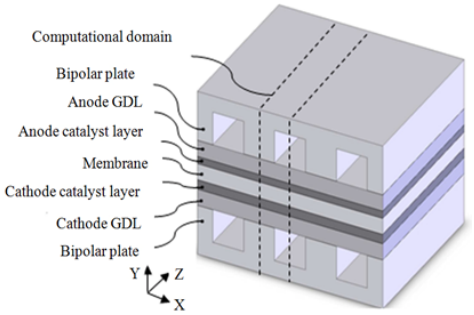

Fig. 1: Schematic of a PEM fuel cell.

Mathematical Model:

The computational domain of model that was employed here is shown in Fig. 1. As it is shown, it is a three-dimensional polymer electrolyte fuel cell with two straight channels in the anode and cathode sides, two bipolar plates, two gas diffusion layers, and membrane layer. Bipolar plates (also known as shoulders) work as current collectors with high electronic conductivity. The middle planes of the flow channels and bipolar plates are assumed as symmetry plane, because the structure of the fuel cell system in this model is supposed to repeat periodically along the x-direction. Hence, here only half the domain is taken into account. This assumption is logical until no cross-flow takes place between the channels that are placed next to each other. The X-Y view of the computational mesh of the base case is shown in Fig. 2.

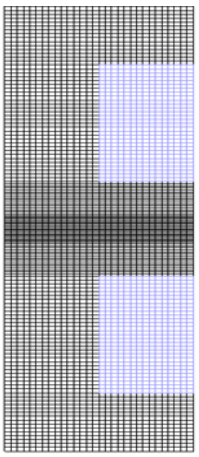

Fig. 2: X-Y view of the Computational mesh of the domain.

Model Assumptions:

The proposed model includes the following assumptions:

(1) The system operates under a steady-state condition.
(2) The gas mixture is an incompressible ideal fluid.
(3) The flow in the flow channels is laminar because of small pressure gradients and flow velocities.
(4) The gas diffusion layers, catalyst layers and membrane are isotropic and homogeneous porous media.
(5) The membrane is considered impassable for reactant gases.

Governing Equations:

The proposed model is based on a single-domain approach for the governing equations, which are applicable for all the sub-domains used. So, at interfaces between the sub-domains of the cell no interfacial conditions are used. According to the preceding assumptions for the model, the governing equations can be written as below:

1) Mass conservation equation

$$\nabla.(\rho\vec{u}) = 0 \tag{1}$$

Where, ρ and $\vec{u}$ are the density of gas mixture and the fluid velocity vector, respectively. Mass source/sink terms are neglected due to the previous assumptions (2) and (3).

2) Momentum conservation equation

$$\frac{1}{(\varepsilon^{eff})^2}\nabla.(\rho\vec{u}\vec{u}) = -\nabla P + \nabla.(\mu\nabla\vec{u}) + S_u \tag{2}$$

Where, ε^{eff} and μ denote the effective porosity inside the porous mediums and the viscosity of the gas mixture, respectively. The source term in the momentum equation, S_u, is used to represent Darcy's drag for flow through porous gas diffusion layers and catalyst layers (Garau, 1998), as:

$$S_u = \frac{\mu}{k}\vec{u} \tag{3}$$

Here, k is the permeability inside porous mediums.

3) Species conservation equation

$$\nabla.(\vec{u}C_k) = \nabla.(D_k^{eff}\nabla C_k) + S_K \tag{4}$$

Where, k denotes the chemical species involving hydrogen, oxygen, nitrogen and water. D_k^{eff} is the effective diffusion coefficient that is used to describe the porosity effects in the porous gas diffusion layers and catalyst layers of species. It is defined by the Bruggeman equation (Meredith, 1960), as:

$$D_k^{eff} = (\varepsilon^{eff})^{1.5} D_k \tag{5}$$

Also, the diffusion coefficient is specified as a function of temperature and pressure by the following correlation (Bird, 1960):

$$D_k = D_k^0 (\frac{T}{T_0})^{3/2} (\frac{P_0}{P}) \tag{6}$$

The species source terms are defined as follows:

$$S_k = \begin{cases} 0 & \textit{Flow channels} \\ 0 & \textit{GDL} \\ -\nabla.(\frac{n_d}{F} I) - \frac{s_k j}{nF} & \textit{Catalyst layers} \\ -\nabla.(\frac{n_d}{F} I) & \textit{Membrane} \\ 0 & \textit{Bipolar plates} \end{cases} \tag{7}$$

4) Charge conservation equation:

$$\nabla.(\sigma_e^{eff} \nabla \phi_e) + S_\phi = 0 \tag{8}$$

Where σ_e and ϕ_e are the ionic conductivity in the membrane (Springer, 1991) and the electrolyte phase potential, respectively. The source term in the charge equation, S_ϕ, in the catalyst layers is equal to exchange current density. In the other sub-layers no source term is needed.

$$\sigma_e = (0.514\lambda - 0.326) e^{1268(\frac{1}{303} - \frac{1}{T})} \tag{9}$$

$$\sigma_e^{eff} = \varepsilon_m^{1.5} \sigma_e \tag{10}$$

Here, λ and ε_m are water content and the volume fraction of the membrane phase in the catalyst layer, respectively. The number of water molecules for each sulfonate group in the membrane is called water content. The water content is defined by the following equation as a function of water activity, α, as:

$$\lambda = \begin{cases} 0.043 + 17.18a - 39.85a^2 + 36a^3 & (a < 1) \\ 14 + 1.4(a-1), & (a > 1) \end{cases} \tag{11}$$

Water activity is defined as:

$$a = \frac{P_{wv}}{P_{Sat}} \tag{12}$$

$$P_{wv} = x_{H_2O} P \tag{13}$$

$$P_{sat} = 10^{-2.1794 + 0.02953(T - 273.17) - 9.1837 \times 10^{-5} (T - 2273.17)^2 + 1.4454 \times 10^{-7} (T - 273)^3} \tag{14}$$

Where, P_{wv} and P_{sat} are water vapor pressure and saturation pressure, respectively, and x_{H_2o} is the mole fraction of water.

5) Energy equation

$$\nabla.(\rho u T) = \nabla.(\lambda_{eff} \nabla T) + S_T \tag{15}$$

Where, λ_{eff} is the effective thermal conductivity, and the source term of the energy equation, S_T, is defined with the following equation:

$$S_T = I^2 R_{ohm} + h_{reaction} + \eta_{an} i_{an} + \eta_{ca} i_c \tag{16}$$

In this equation, R_{ohm} , is the ohmic resistance of the membrane, $h_{reaction}$, is the heat generated thorough the chemical reactions, η_a and η_c , are the anode and cathode overpotentials, which are calculated as:

$$R_{ohm} = \frac{t_m}{\sigma_e} \tag{17}$$

Here, t_m is the membrane thickness.

$$\eta_a = \frac{RT}{\alpha_a F} \ln\left[\frac{IP}{j_{0_a} P_{0_{H_2}}}\right] \tag{18}$$

$$\eta_C = \frac{RT}{\alpha_c F} \ln\left[\frac{IP}{j_{0_c} P_{0_{O_2}}}\right] \tag{19}$$

Where, α_a and α_c , are the anode and cathode transfer coefficients, P_0 , is the partial pressure of hydrogen and oxygen, and j_0 , is the reference exchange current density.

The local current density of the cell is defined as:

$$I = \frac{\sigma_e}{t_m}\{V_{OC} - V_{Cell} - \eta\} \tag{20}$$

Here, V_{oc} is the open circuit voltage, and η is represent the losses.

Water Transport:

In polymer electrolyte fuel cells, the water molecules transport in the membrane is performed by electro-osmotic drag and the molecular diffusion. The water transport through the polymer electrolyte membrane by the H^+ protons is called Electro-osmotic drag mechanism. Also, because of the oxygen reduction reaction in the cathode catalyst layer, water vapor is produced. The following conservation equation determines water transport through the polymer electrolyte membrane:

$$\nabla.(D_{H_2O}^{mem} \nabla C_{H_2O}^{mem}) - \nabla.(\frac{n_d}{F} i) = 0 \tag{21}$$

Where, $D_{H_2O}^{W}$ is the water diffusion coefficient in the membrane and n_d is the water drag coefficient from anode to cathode. The drag coefficient of water is determined as the number of water molecules carried by each hydrogen proton H^+ . The water drag coefficient can be expressed as (Kuklikovsky, A.A, 2003):

$$n_d = \begin{cases} 1 & (\lambda < 9) \\ 0.117\lambda - 0.0544 & (\lambda \geq 9) \end{cases} \tag{22}$$

The water diffusion coefficient in the membrane is defined as a function of the water content of the membrane and is expressed as (Yeo, 1997):

$$D_w^{mem} = \begin{cases} 3.1\times10^{-7}\lambda(e^{0.28\lambda}-1)e^{(-2346/T)} & 0<\lambda\le 3 \\ 4.17\times10^{-8}\lambda(1+161e^{-\lambda})e^{(-2346/T)} & otherwise \end{cases} \quad (23)$$

Boundary Conditions:

In each computational domain boundary conditions have to be used for all variables of interest. All gradients at the y-z plane boundaries of the domain are set to zero because symmetry is adopted in the x-direction.

Uniform temperature and gas species concentrations are adopted at the gas channel inlet. The inlet velocities are defined as:

$$u_{a,in} = \zeta_a \frac{I_{ref}}{2F} A_{MEA} \frac{RT_{a,in}}{P_{a,in}} \frac{1}{X_{H_2,in}} \frac{1}{A_{ch}} \quad (24)$$

$$u_{c,in} = \zeta_c \frac{I_{ref}}{4F} A_{MEA} \frac{RT_{c,in}}{P_{c,in}} \frac{1}{X_{o_2,in}} \frac{1}{A_{ch}} \quad (25)$$

Where, R is the universal gas constant, T_{in} is temperature in the inlet, P_{in} is pressure in the inlet, ζ is the stoichiometric ratio and is defined as the ratio between the amount supplied and the amount required of the reactant on the basis of the reference current density I_{ref}.

At gas-flow channels outlet, only the pressure is being expressed as the electrode pressure.

RESULTS AND DISCUSSION

Model Validation:

In order to validate the proposed model, a series of simulations were performed on the base case using the geometrical and physical parameters presented in tables 1 and 2, respectively, and the resulting polarization curve was compared with the experimental data of Ticianelli *et al*. (1988). As it is shown in Figure 3, the computed polarization curve reveals a good agreement with the experimental data.

Table 1: Geometrical parameters

Parameter	Value [m]
Channel length	0.05
Channel height	1.0×10^{-3}
Channel width	1.0×10^{-3}
shoulder width	1.0×10^{-3}
Electrode thickness	0.23×10^{-3}
Membrane thickness	0.26×10^{-3}

Table 2: Physical and electrochemical parameters

Parameter	Value
Inlet fuel and air temperature	$80°c$
Air side pressure	5 *atm*
Fuel side pressure	3 *atm*
Air stoichiometric flow ratio, ζ_a	3
Fuel stoichiometric flow ratio,ζ_c	3
Relative humidity of inlet gases	100%
Gas phase electrode porosity, ε_g	0.4
Transfer coefficient, anode side, α_a	0.5
Transfer coefficient, cathode side, α_c	1
Ref. exchange current density, cathode $i_{0,a}^{ref}$	0.6
Ref. exchange current density, cathode, $i_{0,c}^{ref}$	4.4×10^{-7} *a/cm*^{2}
Thermal conductivity of the membrane, λ	0.67 *W/m-k*

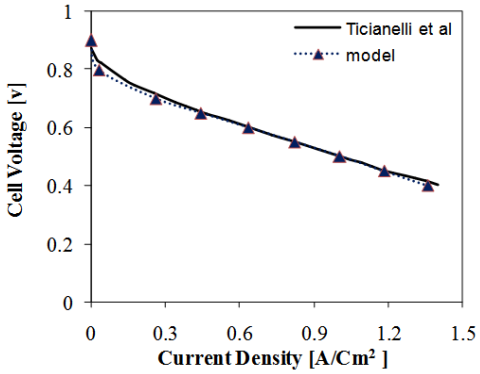

Fig. 3: Measured and predicted cell polarization curves.

Effect of Channel Cross-section:

We carried out simulations for the PEM fuel cell with rectangular and trapezoidal channel cross-sections, which are schematically illustrated in figure 4. Both of the configurations were run with similar boundary conditions and inlet mass flow rates.

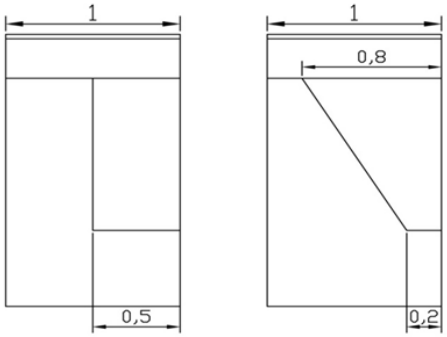

Fig. 4: Cross-sectional view of two geometrical configurations.

The obtained current densities at the cell voltage of V= 0.4 v are displayed in figure 5. The current density for rectangular channel cross-section is higher than the other case.

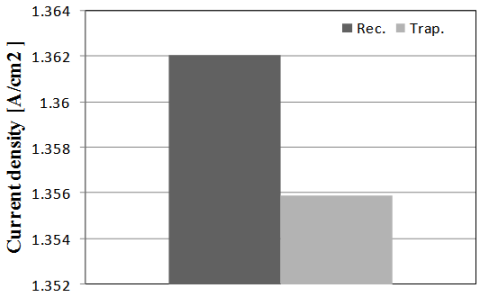

Fig. 5: Average current density obtained for two geometries at V =0.4 v.

Eq.20 shows that the local current density in directly proportional to the local overpotential and membrane conductivity. The local overpotential contains the anode and the cathode overpotentials, which should be decreased in order to increase the local current density. Membrane conductivity is the other effective factor on the local current density that reversely affects the ohmic loss (Eq.17). Each of the losses, which are mentioned above, is investigated separately in the following sections.

Anode Overpotential:

Fig.6 shows the mean values of the anode overpotential for two cases at z=10, which were computed at the interface of the membrane and the anode catalyst layer. The anode concentration loss is lower in the

trapezoidal channel cross-section than the rectangular configuration. With the increase in the interface of the channel and the gas diffusion layer in the trapezoidal case, hydrogen diffuses better over the reacting area and decreases the anode overpotential. It is found that the anode overpotential can be disregarded in PEMFCs (Bird, 1960), which matches with our result.

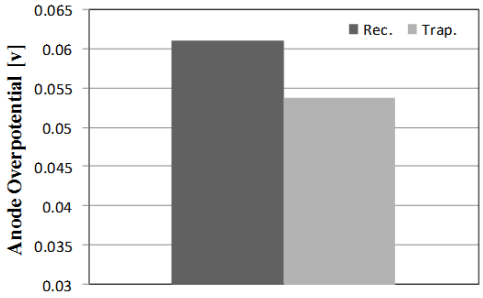

Fig. 6: Anode overpotential at membrane-anode catalyst interface, z=10.

Cathode Overpotential:

At the interface of the membrane and the cathode catalyst layer, the width average values of the cathode overpotential for the two indicated cases are calculated at the channel length of z=10 from inlet. These loss values are shown in figure 7. Similar to the anode side the concentration loss in the cathode electrode is lower in the trapezoidal cross-section.

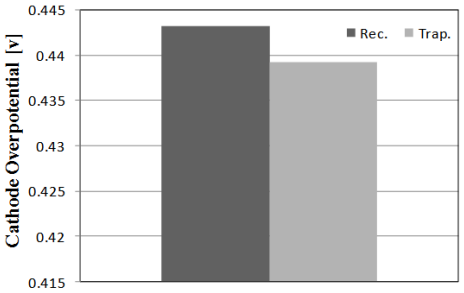

Fig. 7: Cathode overpotential at the membrane-cathode catalyst interface, z=10.

The local cathode loss is presented in Eq.19; partial pressure in this equation is related to the reactant mole fraction. So the cathode overpotential is affected by the oxygen mole fraction. At the section of z=10 in figure 8, the oxygen mole fraction is shown for the rectangular and the trapezoidal geometries at the interface of the cathode catalyst and the membrane. It is observed that the mole fraction is higher in the channel section than the shoulder area, which gives rise to higher water production in the channel area. The produced water in the cathode reacting area blocks the holes of the porous GDL, this circumstance reduces diffusion of the oxygen to the reacting area.

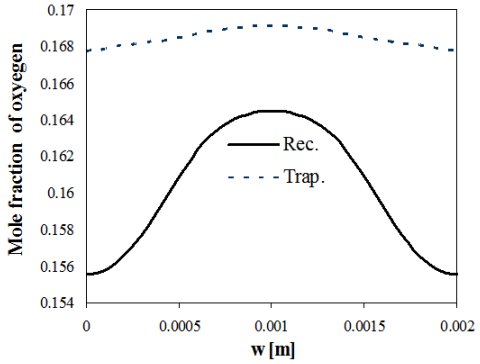

Fig. 8: Oxygen mole fraction at the membrane- cathode catalyst interface, Z=10.

Figure 9a and 9b illustrate contours of the water mole fraction for the two configurations at the cathode gas diffusion layer and the cathode catalyst layer, which are computed at the section of z= 10. As it is shown, the mole fractions are decreased by moving from the shoulder region to the channel region and also by coming down from the catalyst surface to the channel-GDL interface. According to Natarajan and Nguyen (2001) findings, because the produced water over the channel area needs to diffuse a shorter distance along the cathode gas diffusion layer, it rapidly goes away from that region, so the water mole fraction over the channel area is lower in spite of higher water production in that area. The oxygen mole fraction for the rectangular geometry in comparison with the trapezoidal geometry has a lower value in the whole width of the indicated section (figure 8), whereas the water mole fraction in the rectangular configuration is higher than the trapezoidal configuration (figure 9a and 9b). It is obvious that the difference in accumulation of water between those two geometries increases by moving from channel area to the shoulder area. Increasing in water amount leads to overcrowd of more pores in the cathode gas diffusion layer, which results in lower oxygen mole fraction in rectangular case than the other case. With comparing oxygen mole fraction in the two cases, higher difference in the shoulder area than the channel area is reasonable based on the specified reason. More uneven oxygen distribution over the reacting area in the rectangular case than the other case results in higher concentration losses.

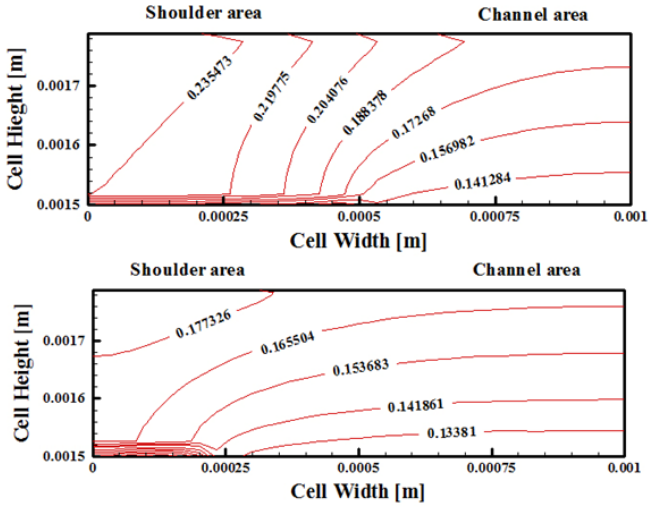

Fig. 9: Water mole fraction distribution at the cathode GDL and catalyst layer, z=10. a) Rectangular case. b) Trapezoidal case.

Ohmic Loss:

Ohmic resistance is calculated according to Eq.17. Ohmic loss is attained form multiplying the ohmic resistance and current density. So ohmic loss is directly related to the membrane thickness, t_m, and local current density, I, and inversely related to the membrane conductivity, σ_e. Figure 10 shows the ohmic loss at the membrane-cathode interface. As it is shown, ohmic loss is higher in the channel area than the shoulder area.

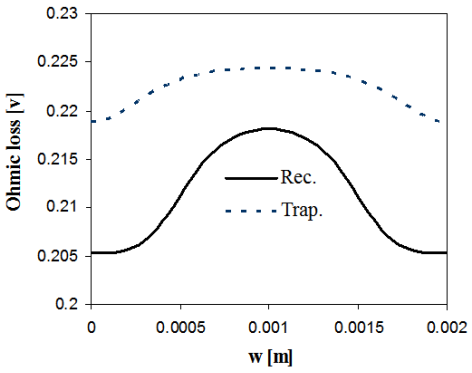

Fig. 10: Comparison of ohmic losses at the membrane–cathode catalyst interface, z=10.

Ohmic loss is mainly controled by the membrane conductivity that is persented in figure 11. It is higher in the shoulder area than the channel area. Eq.11 reveals that, σ_e is dependent on the water content and temperature. Temperature distribution is shown in Figure 12. Constant temprature of the top surface in the anode bipolar plate and the bottom surface in the cathode bipolar plate and also high thermal conductivity of the bipolar plates leads to a lower temprature in the shoulder region than the channel region. Higher temperature in the tarepezoidal cross-section results in a increase in the saturation pressure (Eq.14) and consequently gives rise to a reduction in the water activity. This lower water activity in the trapezoidal cross-section leads to lower water content in this case than the other case. According to the presented reasons,this trend for the membrane conductivity over the reacting area and its lower value in the trapezoidal cross-section is reasonable.

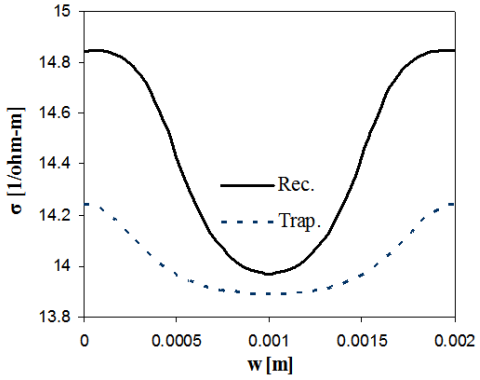

Fig. 11: Comparison of membrane conductivity at the membrane-cathode catalyst interface, z=10.

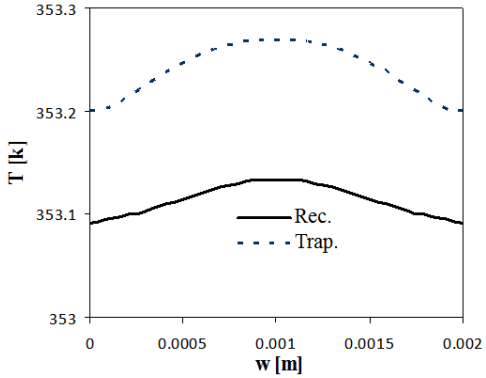

Fig. 12: Temperature distribution at the membrane-cathode catalyst interface, z=10.

The results show that the trapezoidal cross-section leads to a higher ohmic loss compared with the rectangular cross-section.

Conclusions:

In this study, simulations were executed for a polymer electrolyte fuel cell with straight channels in anode and cathode sides. Effect of channel cross-section on the performance of a PEMFC was investigated. Two different geometries with rectangular and trapezoidal channel cross-sections were chosen. The channel cross-sectional area was maintained constant and consequently inlet boundary conditions were the same in the indicated geometries. Current densities at the adjusted cell voltage V=0.4 v were calculated that was higher in the rectangular case. Different types of losses were calculated for the two cases. Trapezoidal configuration showed lower concentration losses in the both anode and cathode sides because this configuration helps the reactants to diffuse more uniformly over the reacting area, and ohmic loss became lower in the rectangular cross-section due to the higher membrane conductivity in it. The overall effect of the indicated losses led to decrease in the current density in the trapezoidal cross-section than the other cross-section in a low cell voltage.

Nomenclature:

a	Water activity
C	Molar concentration (mol/m^3)
D	Mass diffusion coefficient (m^2/s)
F	Faraday constant (C/mol)
I	Local current density (A/m^2)
J	Exchange current density (A/m^2)
K	Permeability (m^2)
M	Molecular weight (kg/mol)
n_d	Electro-osmotic drag coefficient
P	Pressure (Pa)
R	Universal gas constant (J/mol-K)
T	Temperature (K)
t	Thickness
$\vec{u}$	Electrolyte phase potential
V_{cell}	Cell voltage
V_{oc}	Open-circuit voltage
W	Width
X	Mole fraction

Greek Letters:

α	Water transfer coefficient
ε^{eff}	Effective porosity
ρ	Density (kg/m^3)
μ	Viscosity (kg/m-s)
σ_e	Membrane conductivity (1/ohm-m)
λ	Water content in the membrane
ζ	Stoichiometric ratio
η	Overpotential (v)
λ_{eff}	Effective thermal conductivity (w/m-k)
ϕ_e	Electrolyte phase potential (v)

Subscripts and Superscripts:

a	Anode
c	Cathode
ch	Channel
k	Chemical species
m	Membrane
MEA	Membrane electrolyte assembly
ref	Reference value
sat	saturated
w	Water

REFERENCES

Barbir, R., 2005. PEM Fuel Cells: Theory and Practice. Elsevier Academic Press.

Bird, R.B., W.E. Stewart and E.N. Lightfoot, 1960. Transport Phenomena. John Wiley & Sons.

Buchi, F.N. and Günter G. Scherer, 2001. Investigation of the Transversal Water Profile in Nafion Membranes in Polymer Electrolyte Fuel Cells. Journal of Electrochemical Society, 148(3): A183-A188.

Chiang, M.S. and H.S. Chu, 2006. Numerical Investigation of Transport Component Design Effect on a Proton Exchange Membrane Fuel Cell. Journal of Power Sources, 160(1): 340-352.

Ge, S. and B. Yi, 2003. A Mathematical Model for PEMFC in Different Flow Modes. Journal of Power Sources, 124(1): 1-11.

Guvelioglu, G.H., H.G. Stenger, 2005. Computational Fluid Dynamics Modeling of Polymer Electrolyte Membrane Fuel Cells. Journal of Power Sources, 147(9): 95-106.

Garau, V., H. Liu and S. Kakac, 1998. Two-Dimensional Model for Proton Exchange Membrane Fuel Cells. AIChE Journal, 44(11): 2410-2422.

Kuklikovsky, A.A, 2003. Quasi-3D Modeling of Water Transport in Polymer Electrolyte Fuel Cells. Journal of Electrochemical Society, 150 (11):A1432-A1439.

Larminie, J. and A. Dicks, 2003. Fuel Cell Systems Explained. Second ed., John Wiley & Sons, England, pp: 51-52.

Meredith, R.E. and C.W. Tobias, 1960. Advances in Electrochemistry and Electrochemical Engineering 2. Interscience Publishers.

Natarajan, D., T.V. Nguyen, 2001. A Two Dimensional, Two Phase, Multi-component, Transient Model for the Cathode of a Proton Exchange Membrane Fuel Cell Using Conventional Gas Distributors. Journal of Electrochemical Society, 148(12): A1324-A1335.

O'Hayre, R., S.W. Cha, W. Colella and F.B. Prinz, 2006. Fuel Cell Fundamentals. John Wiley & Sons.

Springer, T.E., T.A. Zawodzinski and S. Gottesfeld, 1991. Polymer Electrolyte Fuel cell Model. Journal of the Electrochemical Society, 138(8): 2334-2342.

Sun, L., P.H. Oosthuizen and K.B. McAuley, 2006. A Numerical Study of Channel-to-Channel Flow Cross-over Through the Gas Diffusion Layer in a PEM-fuel-cell Flow System Using a Serpentine Channel with a Trapezoidal Cross-sectional Shape. International Journal of Thermal Sciences, 45(10): 1021-1026.

Ticianelli, E.A., C.R. Derouin, A. Redondo and S. Srinivasan, 1988. Methods of Advance Technology of Proton Exchange Membrane Fuel Cells. Journal of Electrochemical Society, 135(9): 2209-2214.

Yeo, S.W. and A. Eisenberg, 1997. Journal of Applied Polymer Science, 21: 875.